

## Chapter 2

# Optimisation of PLD Parameters

**Abstract** Progress in the fabrication of ZnO-based optoelectronic devices lies in producing reproducible, reliable and stable p-type ZnO films, because of the intrinsic n-type nature of the deposited ZnO films. Hence, for successful conversion of its carriers from n-type to p-type, it is desirable that the deposited ZnO film has as low an electron concentration as possible. Moreover, for the fabrication of optoelectronic devices, the films should have very high optical quality. The growth of highly oriented films with the least strain will offer an added advantage in fabricating these devices. Hence, the deposition parameters of temperature and pressure using pulsed laser deposition (PLD) were optimised keeping these things in mind. A substrate temperature of 650 °C and oxygen pressure of 40 mTorr were found to be optimised growth parameters as it had the lowest carrier concentration of  $1.01 \times 10^{17} \text{ cm}^{-3}$  a reasonably high Hall mobility of  $16.1 \text{ cm}^2 \text{ V}^{-1} \text{ s}^{-1}$  and also had the highest optical quality. Once the PLD parameters were optimised, hydrogen implantation was carried out to see whether it further enhanced the electrical and optical properties of the thin film. While the Van der Pauw Hall measurements did not reveal any significant changes in the electrical characteristics of the thin films, the optical quality of the implanted films was found to increase by two orders of magnitude when compared to the as-deposited sample. Such an enhancement in the optical luminescence of the ZnO thin films may be helpful in fabricating highly efficient ZnO-based devices.

**Keywords** PLD • X-ray diffraction • Atomic force microscopy • Scanning electron microscopy • Van der Pauw Hall • Photoluminescence • Hydrogen implantation • Thermally stimulated current

---

Part of the chapter has been reprinted from [S. Nagar et al. “Increased photoluminescence of hydrogen-implanted ZnO thin films deposited using pulsed laser deposition technique”, *Journal of Luminescence*, Vol. 15, Pg 307–311, 2014 (with permission from Elsevier)]

## 2.1 Introduction

Progress in the fabrication of ZnO-based optoelectronic devices lies in producing reproducible, reliable and stable p-type ZnO films, because of the intrinsic n-type nature of the deposited ZnO films. Hence, for successful conversion of its carriers from n-type to p-type, it is desirable that the deposited ZnO film has as low an electron concentration as possible. Moreover, for the fabrication of optoelectronic devices, the films should have very high optical quality. The growth of highly oriented films with the least strain will offer an added advantage in fabricating these devices.

Deposition of ZnO thin films was carried out using PLD over  $\langle 001 \rangle$  sapphire substrates. A very low lattice mismatch between ZnO and sapphire substrates explains the use of the substrate. In this study, we optimise (i) the substrate temperature and (ii) the oxygen pressure, keeping in mind the above-mentioned requirements for fabrication of devices.

The deposited films were characterised in order to observe the structural, electrical and optical properties of the films with an intention to obtain films with the least strain, defects and carrier concentration and the highest optical efficiency. The structural properties were characterised using XRD and SEM, while the electrical and optical properties were measured with the Van der Pauw Hall technique and PL, respectively.

## 2.2 Temperature Optimisation

### 2.2.1 Experimental Details

ZnO thin films were deposited over  $\langle 001 \rangle$  sapphire substrates using PLD technique. The 99.999% pure ZnO target was ablated using a KrF excimer laser (248 nm with a 20-ns pulse) for the deposition. The energy density and the target-to-substrate distance were maintained at  $1.94 \text{ J cm}^{-2}$  and 5 cm, respectively. To attain uniform deposition and avoid pit formation, the target was rotated at a frequency of 10 Hz, the same as the laser frequency. Prior to deposition, a high vacuum of  $3 \times 10^{-5}$  mTorr was kept in the chamber, and the substrate was degreased by treatment with trichloroethylene (TCE), acetone and isopropyl alcohol (IPA) for 2 min each. The deposition was performed in a high vacuum chamber under a background oxygen pressure of 0.1 mTorr for 25 min by varying the temperature from 400 to 800 °C.

### 2.2.2 Results and Discussion

#### 2.2.2.1 Structural Properties

The X-ray diffraction pattern for the film deposited at 650 °C is as shown in Fig. 2.1. Peaks at 34° and 72° could be clearly seen which corresponds to the  $\langle 002 \rangle$  and  $\langle 004 \rangle$  ZnO peaks which suggest that ZnO films grow with a highly c-axis

**Fig. 2.1** X-Ray Diffraction spectrum of sample deposited at 650 °C, showing the  $\langle 002 \rangle$  and  $\langle 004 \rangle$  ZnO peaks

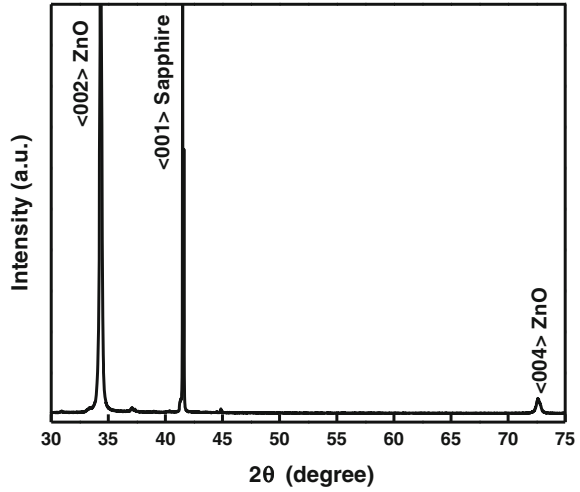
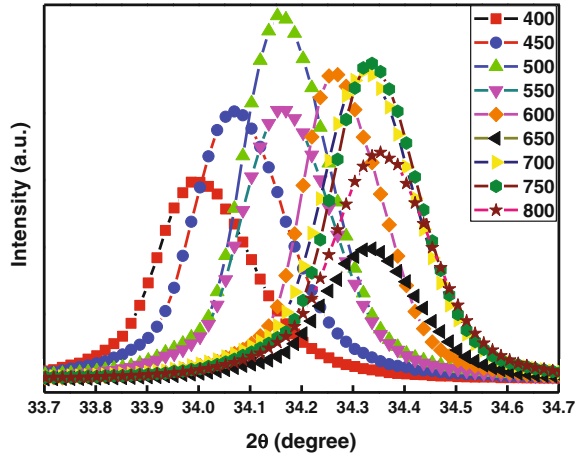


**Fig. 2.2**  $\langle 002 \rangle$  peak positions for different samples



orientation. Absence of other ZnO peaks indicates high crystalline quality of the deposited films which is not the case for films deposited by other techniques like spray pyrolysis or Atomic Layer Deposition (ALD) [102, 103]. It is to be noted that similar spectra was observed for samples deposited at other temperatures. However, a closer examination of the  $\langle 002 \rangle$  peak positions for different samples (Fig. 2.2) displays that the peaks were at different  $2\theta$  angles for different samples. This was due to the lattice strain, calculated by the following equation, caused by the mismatch between the lattice constants of ZnO and sapphire.

**Table 2.1** FWHM values of the  $\langle 002 \rangle$  peak position for samples deposited at different temperatures

Deposition temperature ( $^{\circ}\text{C}$ )	FWHM values ( $^{\circ}$ ) (correct up to 2 decimal places)
800	0.22
750	0.19
700	0.20
650	0.20
600	0.18
550	0.19
500	0.19
450	0.20
400	0.22

$$\text{Strain} = (d_{\text{subs}} - d_{\text{film}})/d_{\text{subs}} \quad (2.1)$$

where  $d_{\text{subs}}$  and  $d_{\text{film}}$  are the  $d$ -spacing of the substrate and the film, respectively. Further, the FWHM values of the ZnO peaks was found to decrease with an increase in substrate temperature until  $650^{\circ}\text{C}$  then increase slightly, followed by further decrease at  $700^{\circ}\text{C}$  (Table 2.1). From the table, it can be seen that the FWHM value for sample deposited at  $650^{\circ}\text{C}$  is not the lowest, but this sample has the least strain and thus serves as a better candidate for device applications.

The surface morphology of the ZnO thin films was studied using SEM. Epitaxial film growth for all the samples was confirmed as no grain formation was observed in the samples. However, due to the lattice strain in the films, cracks were observed in the samples. The cracks seemed to reduce with increase in deposition temperature.

### 2.2.2.2 Electrical Properties

Temperature-dependent (80–300 K) Van der Pauw Hall measurements were performed to study the effect of deposition temperature on the electrical properties of the films (Figs. 2.3 and 2.4). The electron concentration was found to decrease from  $3.1 \times 10^{18} \text{ cm}^{-3}$  at  $800^{\circ}\text{C}$  to  $1.49 \times 10^{18} \text{ cm}^{-3}$  at  $650^{\circ}\text{C}$  followed by further increase to  $4.23 \times 10^{18} \text{ cm}^{-3}$  at  $400^{\circ}\text{C}$  at  $300 \text{ K}$  (Table 2.2). The corresponding Hall mobility was calculated to be 15.7, 24 and  $8.69 \text{ cm}^2 \text{ V}^{-1} \text{ s}^{-1}$ , respectively. Although no major changes in the electron concentration values was found for any of the samples with increase in temperature, a slight increase in the Hall mobility values was identified. As there was no grain formation in the films due to the epitaxial growth of the films, the grain boundary scattering, which is generally affected by temperature, was negligible, thus explaining the increase in mobility values. The measurements revealed that all the films have n-type characteristics.

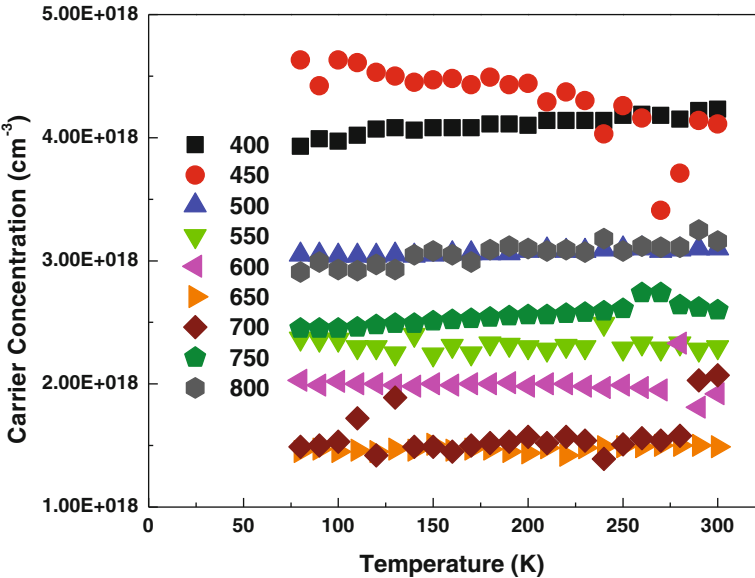


Fig. 2.3 Variation of electron carrier concentration with temperature from 80 K to 300 K

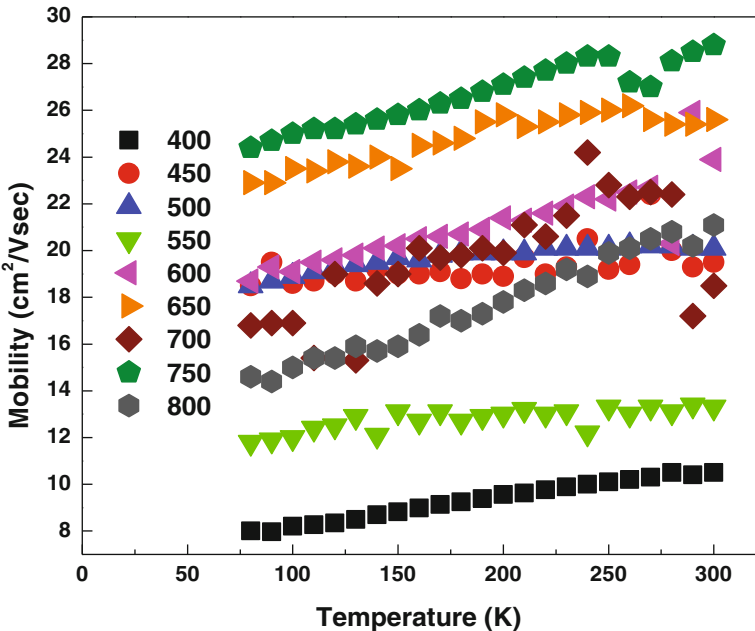
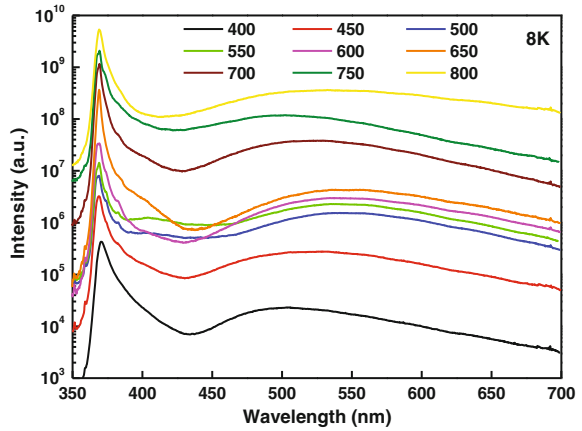


Fig. 2.4 Variation of electron Hall mobility with temperature from 80 to 300 K

**Table 2.2** Electron carrier concentration and Hall mobility values for the obtained samples taken at 300 K

Substrate temperature (°C)	Electron carrier concentration (cm <sup>-3</sup> )	Hall mobility (cm <sup>2</sup> V <sup>-1</sup> s <sup>-1</sup> )
	300 K	300 K
800	$3.16 \times 10^{18}$	21.1
750	$2.6 \times 10^{18}$	28.8
700	$2.07 \times 10^{18}$	18.5
650	$1.49 \times 10^{18}$	25.6
600	$1.92 \times 10^{18}$	23.9
550	$2.3 \times 10^{18}$	13.3
500	$3.1 \times 10^{18}$	20.1
450	$4.11 \times 10^{18}$	19.5
400	$4.23 \times 10^{18}$	10.5

**Fig. 2.5** Low temperature PL spectra (8 K) of the samples showing NBE and deep-level emissions

### 2.2.2.3 Optical Properties

The effect of substrate temperature on the optical properties of the thin films was measured by performing PL measurements. The low-temperature (8 K) PL spectrum of the different samples is shown in Fig. 2.5. A dominant D<sup>0</sup>X emission around 3.36 eV was obtained for all the samples in the NBE region [72, 104]. Other peaks around 3.37, 3.33 and 3.25 eV corresponding to FX, peak due to extended defects and second replica of the LO phonon, respectively, were also observed from the spectrum [72, 105]. Figure 2.6 shows the integrated PL peak intensity of different samples for the D<sup>0</sup>X peak. The PL intensity is first found to decrease at lower temperatures until 550 °C, followed by an increase to reach a maximum at 650 °C. Further increase in the deposition temperature leads to a decrease in the PL intensity. Along with the NBE peaks, deep-level defect peaks centred around 2.4 eV, leading to yellow and green emissions are also detected. These defect peaks

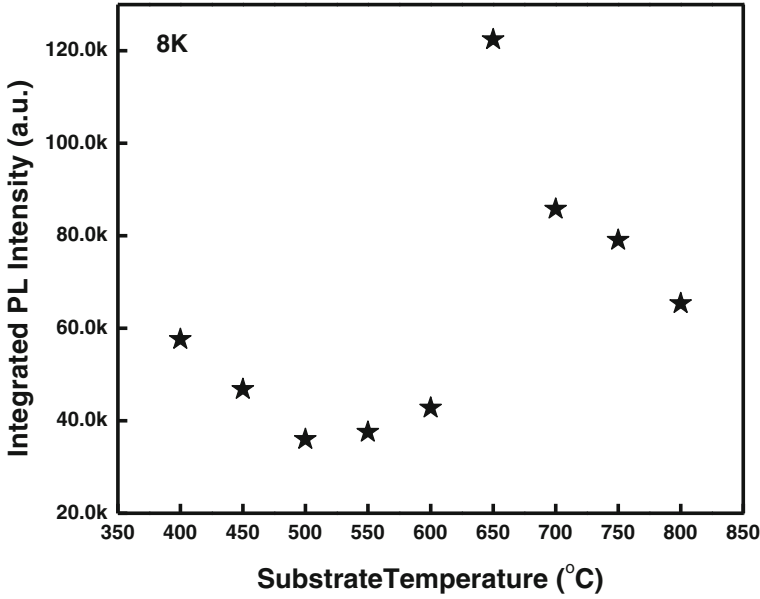


**Fig. 2.6** Integrated PL peak intensity for the D°X peak of all samples taken at 8 K

arise due to intrinsic defects such as  $\text{Zn}_i$  (yellow emission) and  $\text{V}_\text{O}$  (green emission). A closer look at these peaks suggest that the green emission occurs at higher temperatures ( $>650^\circ\text{C}$ ), while the yellow emission is seen at low and intermediate substrate temperatures. However, the intensity of these defect peaks is much lower when compared to the NBE peaks because of the growth of stoichiometric thin films from PLD which is not the case for films grown by other methods [106, 107].

Figure 2.7 shows the temperature-dependent spectrum for a sample deposited at  $650^\circ\text{C}$ . A dominant D°X and a FX shoulder peak are observed at lower temperatures, as mentioned above. At higher temperatures, the FX peak starts to dominate the D°X peak. The peak intensities of FX and D°X with temperature are shown in Fig. 2.8. While the D°X peak diminishes with temperature and vanishes above 150 K, the FX peak intensity first increase and then starts to decrease. The thermal dissociation of bound excitons into free excitons at higher temperatures leads to such an observation [108]. Decrease of the FX peak with temperature  $>150\text{ K}$  is due to the increase in the number of defects with temperature. The evolution of the PL peak energies for the FX and D°X with temperature is shown in the inset of Fig. 2.8. The band gap shrinkage of ZnO is calculated by fitting the temperature dependence of FX peak with temperature using Varshni's equation:

$$E_g(T) = E_g(0) - \alpha T^2 / (T + \beta) \quad (2.2)$$

where  $E_g(0)$  is the band gap of ZnO at  $T = 0\text{ K}$ , and  $\alpha$  and  $\beta$  are the fitting parameters calculated to be  $7 \times 10^{-4}\text{ eV K}^{-1}$  and 515 K, respectively. The band

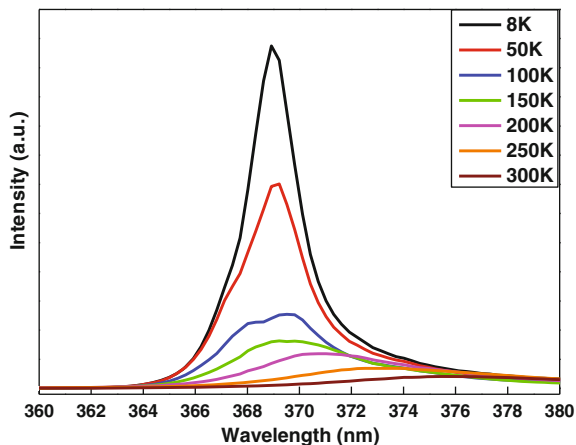
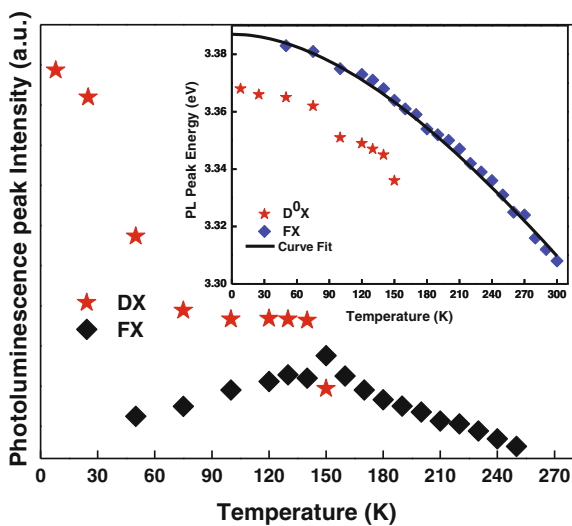


**Fig. 2.7** Temperature-dependent Photoluminescence spectrum for the sample deposited at 650 °C

**Fig. 2.8** PL peak intensity variation with temperature for the FX and D<sup>0</sup>X peaks deposited at 650 °C. *Inset* temperature dependence using Varshni's law



gap of the ZnO film is found to be 3.387 eV, which is in agreement with previously reported values [72, 109].

### 2.2.3 Conclusion

To summarise, PLD technique was used to deposit ZnO thin films over  $\langle 001 \rangle$  sapphire substrates by varying the substrate temperature from 400 to 800 °C. XRD



and SEM results confirmed deposition of highly c-axis-oriented  $\langle 002 \rangle$  epitaxial ZnO films for all the samples. Temperature-dependent Van der Pauw Hall measurements were carried out in order to achieve the optimised sample having the lowest electron carrier concentration and high mobility values for obtaining better p-type films in future. The sample deposited at 650 °C was found to give the lowest carrier concentration of  $1.49 \times 10^{18} \text{ cm}^{-3}$  and a high Hall mobility value of  $24 \text{ cm}^2 \text{ V}^{-1} \text{ s}^{-1}$ . Temperature-dependent PL measurements were carried out to study the optical properties of the thin films and also to attain a film with highest optical quality. Sample deposited at 650 °C was found to be the optimum sample as it had the lowest strain, carrier concentration, a reasonably high Hall mobility value and the best optical quality. As the substrate temperature increases, the ZnO atoms get sufficient energy to diffuse across the substrate, thus resulting in much uniform and high-quality film. However, increasing the substrate temperature too high results in out-diffusion of the ZnO atoms from the surface of the substrate which again degrades the quality of the film. It can be noticed from the various structural, electrical and optical properties that at 650 °C, the ZnO atoms get sufficient energy to diffuse across the substrate uniformly without out diffusing from the surface, thus resulting in the optimised parameters.

## 2.3 Pressure Optimisation

Once the temperature of deposition was optimised, it was required that the oxygen pressure is also optimised so that the carrier concentration becomes minimal along with increased optical luminescence observed from PL spectra. For this purpose, ZnO thin films were deposited over  $\langle 001 \rangle$  sapphire substrates using the same energy density, target-to-substrate distance and deposition time as mentioned in Sect. 2.2.1. The optimised substrate temperature of 650 °C was used for deposition. The oxygen pressure in this case was varied from 0.1 to 60 mTorr.

### 2.3.1 Results and Discussion

#### 2.3.1.1 Structural Properties

XRD results verify the deposition of (002) ZnO thin films with peaks around  $2\theta$  angle of  $34^\circ$  and  $72^\circ$  corresponding to the  $\langle 002 \rangle$  and  $\langle 004 \rangle$  ZnO peaks (Fig. 2.9). The (002) peak shows a shift in position for the various samples, which may be due to the strain developed in the films. The strain in the films has been calculated using Eq. 2.1 and has been plotted for different samples (Fig. 2.10). It is observed that the strain first increases with oxygen pressure up to 10 mTorr, followed by a decrease to attain a minimum value at 40 mTorr. Upon further increasing the oxygen pressure, the strain is found to increase.

**Fig. 2.9** XRD image of the sample deposited at 40 mTorr showing the  $\langle 002 \rangle$  and  $\langle 004 \rangle$  ZnO peaks. *Inset* shows the  $\langle 002 \rangle$  peak positions of all the samples

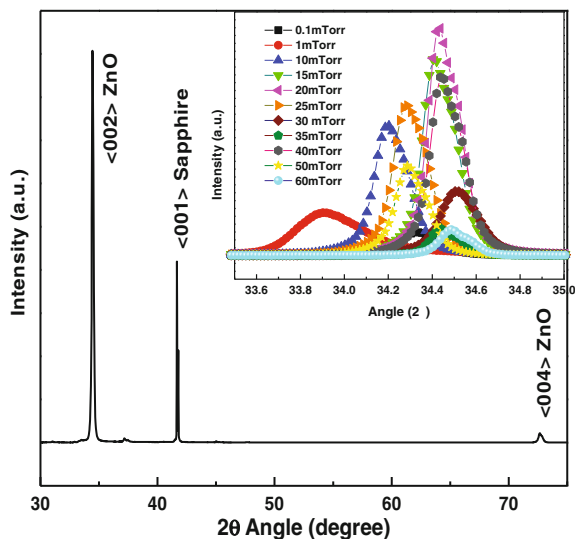
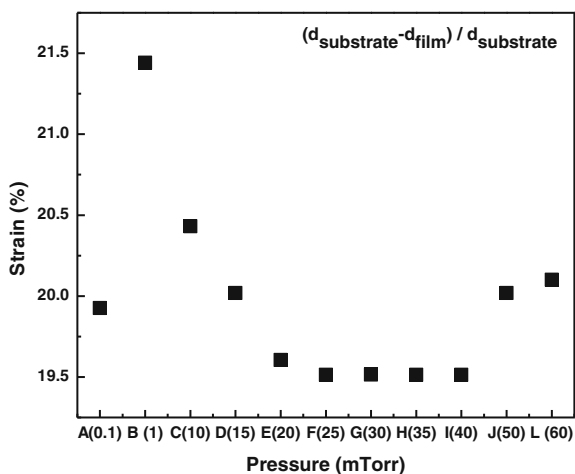


**Fig. 2.10** Variation of lattice strain of ZnO thin films with oxygen pressure



SEM images of the ZnO surface are shown in Fig. 2.11. As the oxygen pressure is increased, grain formation starts to take place. Moreover, the grains are not continuous at lower oxygen pressure (up to 15 mTorr). When the pressure is further increased, the grains grow denser continuously, corresponding to the high quality of the films. However, increasing the pressure beyond 40 mTorr again leads to less dense films and discontinuous grains. A possible reason might be the collisions of the atoms at high pressure during deposition.

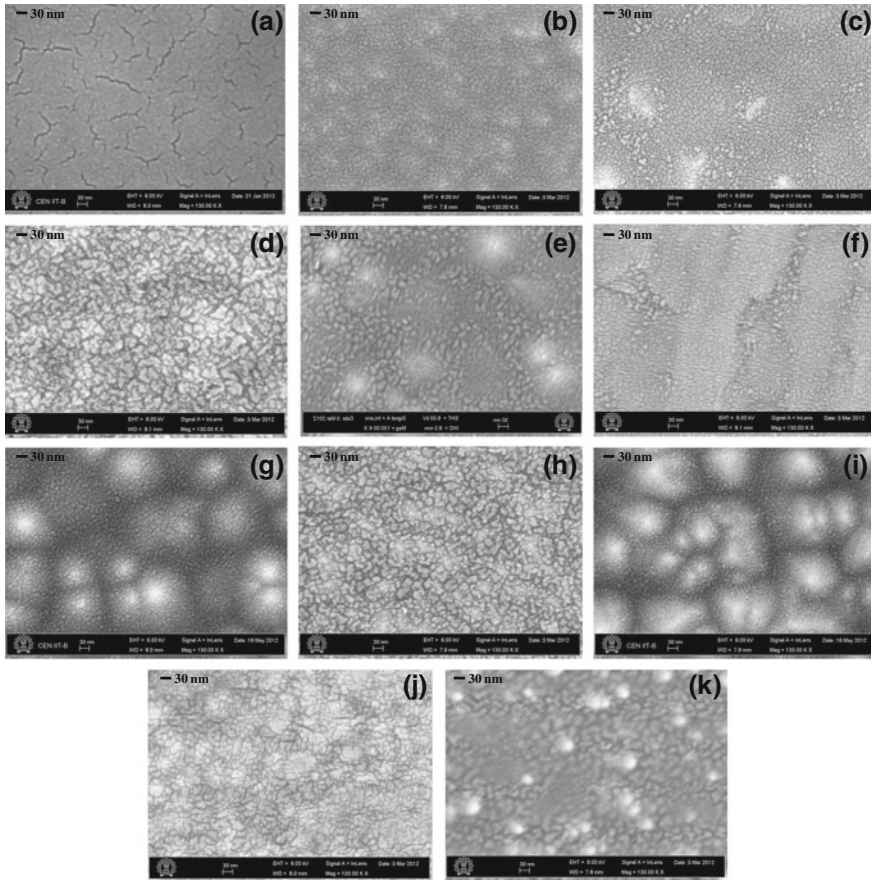


**Fig. 2.11** Scanning electron microscopy (SEM) images of different samples: **a** 0.1, **b** 1, **c** 10, **d** 15, **e** 20, **f** 25, **g** 30, **h** 35, **i** 40, **j** 50 and **k** 60 mTorr, respectively

### 2.3.1.2 Electrical Properties

Temperature-dependent (80–300 K) Van der Pauw Hall measurements were performed to study the electrical properties of the ZnO thin films (Figs. 2.12 and 2.13). Table 2.3 shows the carrier concentration and Hall mobility values at 80 and 300 K. The electron carrier concentration decreases with increase in oxygen pressure, because the amount of  $V_O$  reduces as the pressure increases. However, at higher oxygen pressures (>40 mTorr), the value again increases by an order of magnitude. This may be because less energy is transferred to the substrate due to increased collision among atoms. The Hall mobility values also decrease with pressure until 25 mTorr, after which it starts increasing to gain a sufficiently high value of  $16.1 \text{ cm}^2/\text{V s}$ . The high mobility value at 0.1 mTorr may be due to the lack of grain formation in the sample, leading to negligible grain boundary scattering. In

**Fig. 2.12** Variation of carrier concentration with temperature for various samples

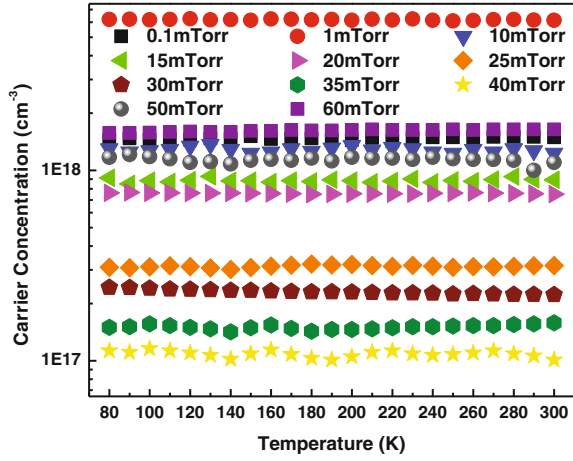
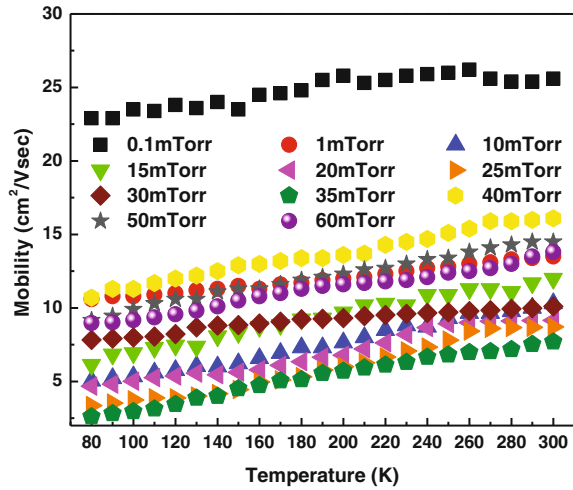


**Fig. 2.13** Variation of Hall mobility with temperature for different samples



this case, too, the variation of carrier concentration with temperature is not observed. However, the Hall mobility tends to show an increase in value with temperature.

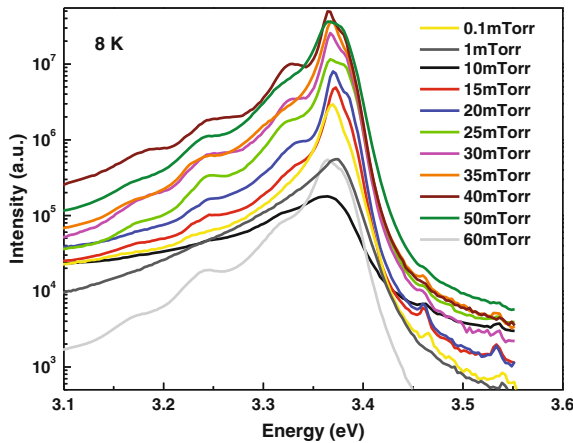
### 2.3.1.3 Optical Properties

Figure 2.14 shows the PL spectra of different samples taken at 8 K of the NBE region. A dominant D°X peak is visible for all the samples around 3.36 eV, along with FX peak at 3.37 eV. The other peaks at 3.33 and 3.25 eV are due to extended defects and LO-phonon replica [72, 104, 105]. Deep-level defect peaks around

**Table 2.3** Carrier concentration and Hall mobility values for the obtained samples at 80 and 300 K

Pressure (mTorr)	Carrier concentration ( $\text{cm}^{-3}$ )		Hall mobility ( $\text{cm}^2/\text{V s}$ )	
	80 K	300 K	80 K	300 K
0.1	$1.45 \times 10^{18}$	$1.49 \times 10^{18}$	24	25.6
1	$6.2 \times 10^{18}$	$6.14 \times 10^{18}$	10.6	13.5
10	$1.3 \times 10^{18}$	$1.23 \times 10^{18}$	5.05	10.3
15	$9.12 \times 10^{17}$	$8.92 \times 10^{17}$	6.14	12
20	$7.72 \times 10^{17}$	$7.5 \times 10^{17}$	4.67	9.15
25	$3.1 \times 10^{17}$	$3.16 \times 10^{17}$	3.36	8.71
30	$2.43 \times 10^{17}$	$2.2 \times 10^{17}$	7.83	10.2
35	$1.5 \times 10^{17}$	$1.58 \times 10^{17}$	2.61	7.7
40	$1.13 \times 10^{17}$	$1.01 \times 10^{17}$	10.7	16.1
50	$1.17 \times 10^{18}$	$1.1 \times 10^{18}$	9.15	14.5
60	$1.57 \times 10^{18}$	$1.64 \times 10^{18}$	8.97	13.8

**Fig. 2.14** PL spectra of the samples taken at 8 K showing NBE transition



2.5 eV are also observed in the samples, although the intensity of the peak is quite low when compared to the NBE peak. This suggests that the ZnO films thus grown are of high quality. The integrated PL peak intensity for D°X peak of different samples is shown in Fig. 2.15. The intensity first decreases with pressure until 40 mTorr, followed by an increase, to attain a highest value at 40 mTorr oxygen pressure. The increased oxygen available during deposition causes fewer defects related to  $V_{\text{O}}$ , causing the film to be of higher quality. However, increasing the oxygen pressure further leads to increased collision among atoms, thus reducing the peak intensity.

The temperature-dependent spectra for a sample grown at a pressure of 40 mTorr are shown in Fig. 2.16. A dominant D°X peak is observed at lower

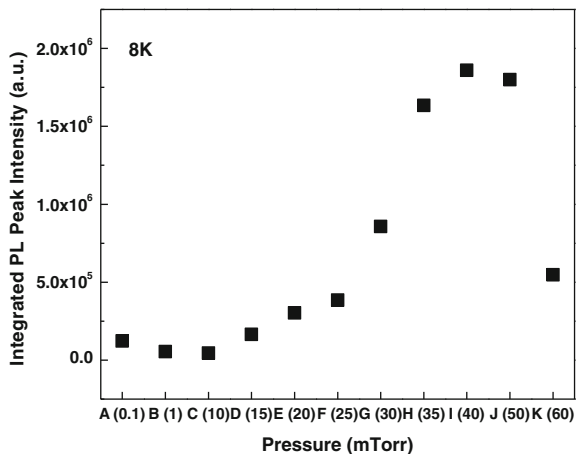


**Fig. 2.15** Integrated PL peak intensity at 8 K for the  $D^{\circ}X$  peak of all samples

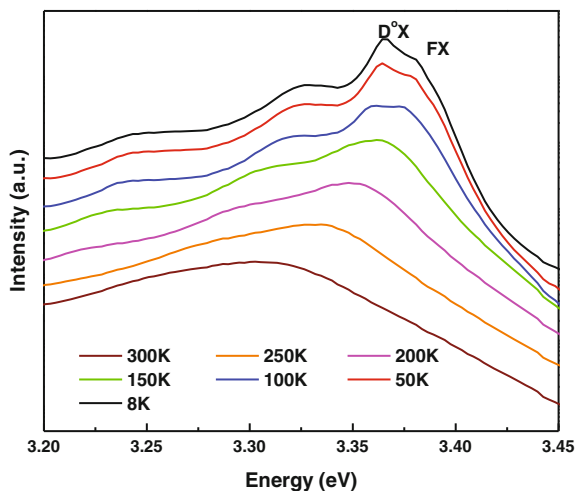
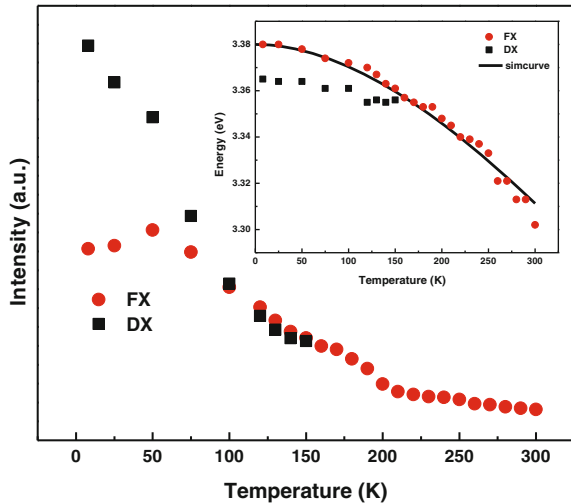


**Fig. 2.16** Temperature-dependent PL spectra for the sample grown at 40 mTorr

temperatures with an FX shoulder. Enhanced thermal dissociation of bound exciton to FX leads to domination of FX peak over  $D^{\circ}X$  peak with temperature [108]. Figure 2.17 shows the FX and  $D^{\circ}X$  PL peak intensities with temperature. A rapid decrease in the  $D^{\circ}X$  peak is observed, which vanishes entirely beyond 150 K. The FX peak, on the other hand, first increases up to 50 K, after which it starts to decrease. Inset of Fig. 2.17 shows the evolution of the PL peak energy with temperature for the  $D^{\circ}X$  and FX peaks, which can be fitted using Eq. 2.2.

**Fig. 2.17** Variation of PL peak intensities with temperature for the FX and D°X peaks for sample deposited at 40 mTorr. *Inset* temperature dependence using Varshni's law



### 2.3.2 Conclusion

ZnO films were deposited over  $\langle 001 \rangle$  sapphire substrates at an optimised temperature of 650 °C in different oxygen pressure. Highly c-axis-oriented  $\langle 002 \rangle$  epitaxial films were obtained for all the samples. The sample deposited at a pressure of 40 mTorr was found to have the lowest strain and very high grain density, as observed from SEM. Temperature-dependent Van der Pauw Hall measurements within a range of 80–300 K were obtained to achieve an optimal sample with low carrier concentration and high mobility values. The lowest concentration of  $1.01 \times 10^{17} \text{ cm}^{-3}$  at 300 K was obtained with a corresponding Hall mobility of  $16.1 \text{ cm}^2 \text{ V}^{-1} \text{ s}^{-1}$  for a sample deposited at an oxygen pressure of 40 mTorr. Temperature-dependent PL spectra were also examined to study the optical behaviour of the films and to obtain a sample with high optical quality. The oxygen pressure of 40 mTorr yielded an optimal sample with the least strain and carrier concentration, along with a high Hall mobility value and the best optical quality. It is a well-known fact that an increase in the pressure of a chamber reduces the mean free path of the particle. Hence, at low pressures, the mean free path is more which corresponds to the atoms in the plume travelling more distance, and thus, the plume does not converge at the substrate leading to non-uniformity and degraded film quality. Similarly, too high a pressure causes to plume to converge well before the substrate, and hence, most of the atoms are unable to get deposited on the film again leading to poor film quality and non-uniformity. From the results obtained through the various characterisation techniques, it is believed that at an oxygen pressure of 40 mTorr, the plume converges at the substrate leading to high-quality films.

## 2.4 Hydrogen Ion Implantation

Once the temperature and oxygen pressure was optimised, hydrogen ion implantation was carried out to see whether it further enhanced the electrical and optical properties of the thin film. An approach similar to the one described in Sect. 2.2.1 was applied to deposit ZnO thin films over  $\langle 001 \rangle$  sapphire substrate. However, here, the optimised values of temperature and oxygen pressure (650 °C and 40 mTorr, respectively) were used during the deposition time to obtain Sample A.

The films thus deposited were subjected to hydrogen ion implantation using Low-Energy Accelerator Facility (LEAF) at Bhabha Atomic Research Centre (BARC), Mumbai, India. Energy of 50 keV with a dose of  $5 \times 10^{12}$  ions/cm<sup>2</sup> was used for implantation. Thus, Sample H1 was obtained. As implantation leads to defects in the films, Sample H1 was subsequently rapid thermal annealed at 750, 800, 850 and 900 °C in oxygen ambient for 30 s to produce Samples H2–H5, respectively. RTP was performed on Sample A at the same temperatures and using the same annealing parameters (samples B to E) to compare them with the implanted samples.

### 2.4.1 Results and Discussion

#### 2.4.1.1 Structural Properties

XRD was performed on the obtained samples to study the effect of hydrogen implantation and subsequent annealing on the structural properties of the thin films (Fig. 2.18). The results confirm the deposition of highly c-axis-oriented  $\langle 002 \rangle$  ZnO films for all the samples. No other peaks have been found in the XRD peaks, which suggest that ZnO preferentially grow in the  $\langle 001 \rangle$  direction due to its lowest surface free energy. A closer look at the  $\langle 002 \rangle$  peak for the different samples shows that the Samples H1–H5 are at a higher  $2\theta$  angle as compared to Sample A. The strain developed due to the hydrogen implantation and subsequent annealing causes this effect (Fig. 2.19). The strain was found to increase for Sample H1, which is due to the implantation-related defects. The reduction of defects on annealing leads to lower strain in these samples, although the strain is still higher when compared to Sample A.

#### 2.4.1.2 Electrical Properties

Room temperature Van der Pauw Hall measurements were taken in order to visualise the effect of implantation on the electrical properties on the thin films (Table 2.4). A decrease in the carrier concentration and Hall mobility is observed for Sample H1 as compared to Sample A. The heating caused by hydrogen



**Fig. 2.18** XRD spectra of the different samples showing the  $\langle 002 \rangle$  ZnO peak. The peak shifts for the implanted samples are clearly visible

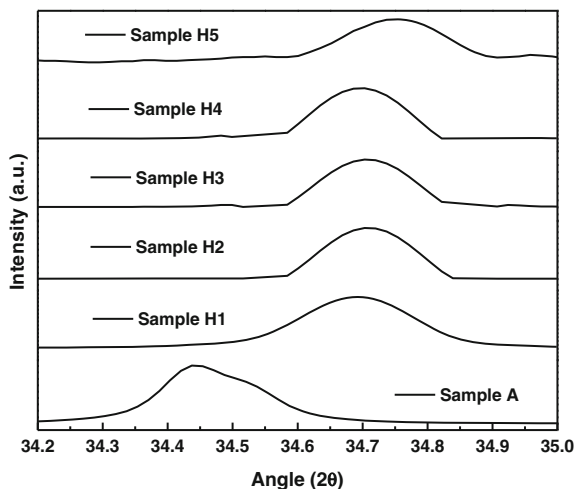
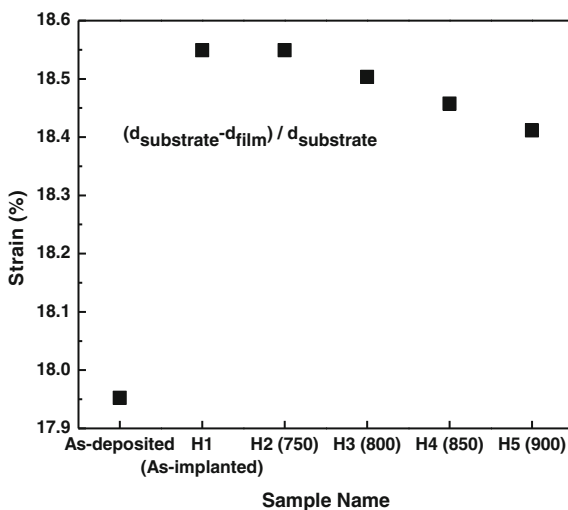


**Fig. 2.19** Strain on the ZnO films due to implantation



implantation may have reduced the intrinsic defects in the sample, leading to lower concentration. However, the increased number of atoms in the films leads to higher scattering, thus reducing the Hall mobility. Upon annealing the samples, at higher temperatures, the carrier concentration and Hall mobility start to increase.

Hall measurements were obtained for Samples B to E to check whether hydrogen ions have any effect on the electrical properties of the thin films. Interestingly, hydrogen ions was found to have no effect on the electrical properties of the films, as the carrier concentration and Hall mobility values of Samples H2–H5 are similar to those of Samples B–E, respectively. The increase in the carrier concentration and Hall mobility of the annealed samples are only due to the

**Table 2.4** Carrier concentration, Hall mobility and conductivity of different sample at 300 K

Sample name	Carrier concentration ( $\text{cm}^{-3}$ )		Hall mobility ( $\text{cm}^2/\text{V s}$ )	
	Unimplanted	Implanted	Unimplanted	Implanted
As-deposited	$1.01 \times 10^{17}$		16.1	
As-implanted	NA	$4.5 \times 10^{16}$	NA	8.86
Annealed at 750 °C	$1.13 \times 10^{17}$	$1.24 \times 10^{17}$	18.3	33.9
Annealed at 800 °C	$3.35 \times 10^{17}$	$2.37 \times 10^{17}$	23.2	21.9
Annealed at 850 °C	$5.75 \times 10^{17}$	$8.85 \times 10^{17}$	60.6	54.4
Annealed at 900 °C	$1.07 \times 10^{18}$	$1.14 \times 10^{18}$	67.5	61.3

Reprinted from S. Nagar et al. "Increased photoluminescence of hydrogen-implanted ZnO thin films deposited using pulsed laser deposition technique", *Journal of Luminescence*, Vol. 15, pp. 307–311, 2014; with permission from Elsevier

reduction of the intrinsic defects of the films due to heat treatment. However, in all cases, the films demonstrated n-type behaviour which was obvious as hydrogen acts as donor in ZnO thin films [110–113].

### 2.4.1.3 Optical Properties

Low-temperature PL measurements of the obtained samples were executed in order to determine the optical properties of the implanted ZnO thin films (Fig. 2.20). A dominant donor-bound exciton ( $\text{D}^\circ\text{X}$ ) peak around 3.36 eV and a shoulder around 3.37 eV corresponding to the FX peak were observed for all the samples, which further confirms the n-type behaviour of the samples. The peaks corresponding to the extended defects due to implantation and the second LO-phonon replica of the  $\text{D}^\circ\text{X}$  peak around 3.33 and 3.22 eV, respectively, were also observed in Samples H2–H6 [72, 104, 105]. Deep-level defect peaks around 2.5 eV, corresponding to defects such as  $\text{Zn}_i$ ,  $\text{V}_\text{O}$  and implantation-related defects, were also observed for all the samples. However, the intensity of this peak is substantially weak when compared with the NBE peak intensity. This suggests that the ZnO films are of very high quality.

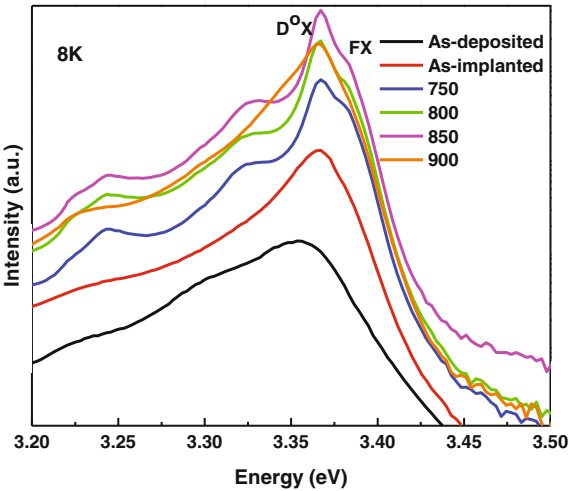
Temperature-dependent PL spectrum of different samples was performed to calculate the thermal activation energy of the samples using Eq. 2.3 (Table 2.5). Figure 2.21 shows the integrated PL peak intensity of the  $\text{D}^\circ\text{X}$  peak for various samples with respect to temperature.

$$I = I_0 * (1 + \exp(-E_A/kT)) \quad (2.3)$$

where  $I$  and  $I_0$  are the integrated PL peak intensity at temperature  $T$  K and 8 K,  $E_A$  is the activation energy and  $k$  is the Boltzmann constant.

The activation energy was found to decrease for Sample H1 due to the increased number of defects caused by implantation. On annealing the samples, the activation energy increases marginally with temperature. However, the activation energy is

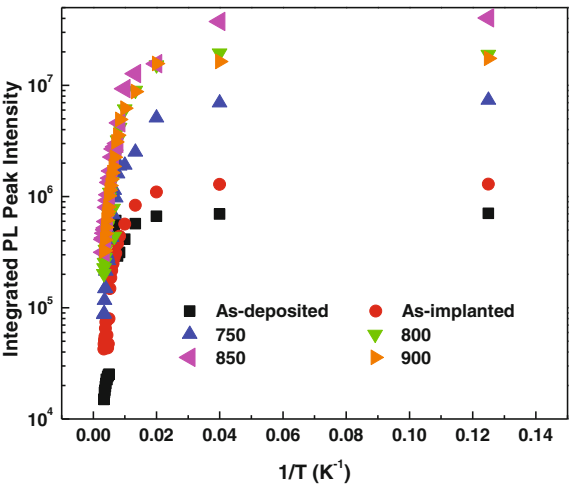
**Fig. 2.20** PL spectra of different samples taken at 8 K (Reprinted from S. Nagar et al. “Increased photoluminescence of hydrogen-implanted ZnO thin films deposited using pulsed laser deposition technique”, *Journal of Luminescence*, Vol. 15, pp. 307–311, 2014; with permission from Elsevier)



**Table 2.5** Thermal activation energy for different samples

Sample name	Thermal activation energy (meV)
As-deposited	66.7
As-implanted	26.5
Annealed at 750 °C	36.98
Annealed at 800 °C	38.6
Annealed at 850 °C	40.5
Annealed at 900 °C	41

**Fig. 2.21** Integrated PL peak intensity with respect to temperature for different samples



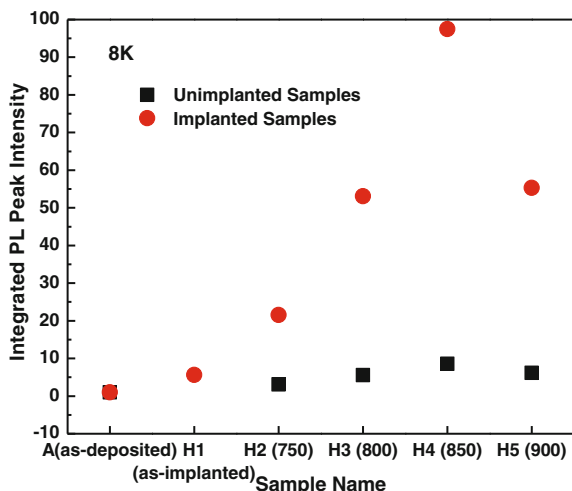


**Fig. 2.22** Photoluminescence (PL) peak intensity at 8 K for unimplanted and implanted samples for the D°X peak (Reprinted from S. Nagar et al. “Increased photoluminescence of hydrogen-implanted ZnO thin films deposited using pulsed laser deposition technique”, *Journal of Luminescence*, Vol. 15, pp. 307–311, 2014; with permission from Elsevier)

still lower than that of Sample A. The formation of shallow donor levels owing to hydrogen implantation leads to lower activation energy in Samples H2–H6 [110–113].

Figure 2.22 illustrates the NBE PL peak intensity for the implanted and unimplanted samples. Notably, the figure shows an obvious increase in the NBE PL peak intensity for the unimplanted sample, with increase in annealing temperature, due to the reduction of defects. A sample annealed at 850 °C demonstrated the highest enhancement of up to nine times that of Sample A. On the other hand, for the implanted sample (Sample H1), the NBE PL peak intensity improved by a factor of four. When the implanted samples were annealed at higher temperatures, the intensity further increased up to 850 °C. When the annealing temperature further increased, the peak intensity reduced, though remaining quite high. The intensity of Sample H4 is as high as 100 times that of Sample A. This result shows that hydrogen implantation and subsequent annealing had some effect on the optical properties of the thin films.

While implantation did not affect the electrical properties of the thin films, their optical properties revealed much improvement in terms of optical output. To understand the reason behind such a behaviour, thermally stimulated current (TSC) was undertaken to understand about the effect of implantation on the defect traps in the ZnO thin films (Fig. 2.23). In TSC measurements, the electron and hole traps are filled by illumination at low temperatures and by subsequent warming the sample in dark while recording the current due to the thermal emission of carriers

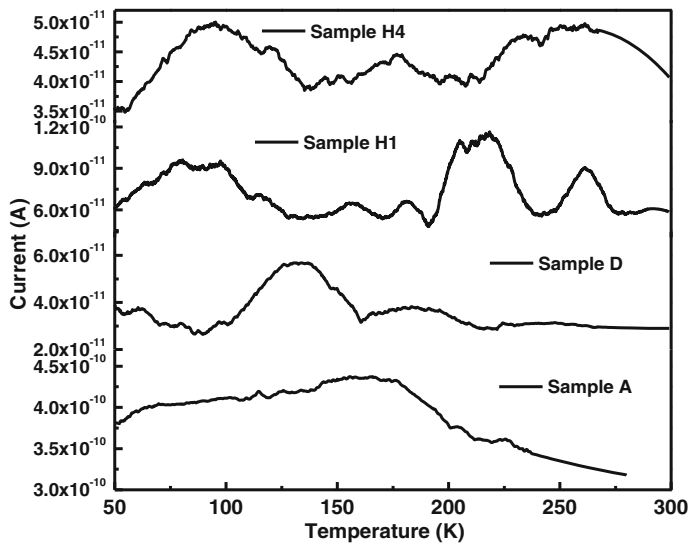


**Fig. 2.23** Thermally stimulated current spectra of Samples A, D, H1 and H4 (Reprinted from S. Nagar et al. “Increased photoluminescence of hydrogen-implanted ZnO thin films deposited using pulsed laser deposition technique”, *Journal of Luminescence*, Vol. 15, pp. 307–311, 2014; with permission from Elsevier)

from the traps [114]. All the samples were first cooled down from room temperature to 8 K, during which the dark current was measured with respect to temperature.

Illumination, for trap filling at 8 K, was performed with a xenon lamp for 30 min. The TSC current was then subsequently measured while warming up at a rate of 5 K/min under a bias of 2 V. A TSC peak around 162 K is observed for the as-deposited sample, which is resolved into two peaks upon annealing at 132 and 185 K. Although TSC measurements cannot reveal the exact nature of the trap, it is believed that these peaks are due to  $V_O$ , as they have activation energy in the range of 0.25–0.33 eV calculated from Eq. 2.4 [114–117].

$$E_T = kT_m \ln(T_m^4/\beta) \quad (2.4)$$

where  $E_T$  is the activation energy of a related trap,  $T_m$  is the peak temperature for the particular trap and  $\beta$  is the heating rate. Upon implantation and subsequent annealing, three other peaks at 87, 215 and 261 K are observed along with relatively small peaks around 160 and 185 K. The exact origins of these peaks are still unknown, but the hydrogen implantation provides clues to the origins of these traps. As the electrical properties of the films do not change even after annealing, it may be possible that these traps are electrically inactive. However, during PL measurements, the trapped electrons are released due to laser illumination, giving rise to increased PL intensity in these peaks. Such an enhanced optical luminescence in ZnO films can be utilised to fabricate devices with very high optical efficiency.

### 2.4.2 Conclusion

The effects of hydrogen implantation at a low energy of 50 keV and of subsequent annealing on the PLD-deposited ZnO thin films were investigated. A strong c-axis-oriented  $\langle 002 \rangle$  ZnO films have been deposited in each case. However, the strain developed in the films due to implantation caused the peaks to shift to higher  $2\theta$  angles. Van der Pauw Hall measurements did not show any change in the carrier concentration and Hall mobility of the implanted and annealed samples, compared to as-annealed samples. While the PL results showed a dominant D<sup>°</sup>X for all the samples, a significant increase in the PL emission ( $\times 4$  and  $\times 100$  times) was observed for the implanted sample and sample annealed at 850 °C. The formation of hydrogen-related traps due to implantation has caused an increased PL emission from the sample. To the best of our knowledge, this report is one of the first in which an improvement in the luminescence intensity has been observed. Such an enhancement in the optical luminescence of the ZnO thin films may be helpful in fabricating highly efficient ZnO-based devices.

Optimisation of ZnO Thin Films

Implants, Properties, and Device Fabrication

Nagar, S.; Chakrabarti, S.

2017, XIX, 83 p. 67 illus., 36 illus. in color., Hardcover

ISBN: 978-981-10-0808-5